Am J Transl Res 2026;18(7):5891-5912
www.ajtr.org /ISSN:1943-8141/AJTR0172560

Original Article

Iron-lipid crosstalk in the progression from gestational diabetes to preeclampsia: proteomic discovery and targeted validation

Wenni Zhou[1*], Dandan Chen[1*], Rong Chen[1], Caixia Li[1], Yan Xie[2], Zhongping Cheng[1]

[1]Department of Obstetrics and Gynecology, Shanghai Tenth People's Hospital, School of Clinical Medicine of Nanjing Medical University, Shanghai, China; [2]Medical Center of Diagnosis and Treatment for Cervical Diseases, The Obstetrics and Gynecology Hospital of Fudan University (Shanghai Red House Ob and Gyn Hospital), Shanghai, China. [*]Equal contributors.

Received March 10, 2026; Accepted May 27, 2026; Epub July 15, 2026; Published July 30, 2026

Abstract: Objectives: The pathogenesis underlying the transition from gestational diabetes mellitus to pre-eclampsia (GDM-PE) has not been fully elucidated. Here, we performed plasma proteomic profiling to analyze the interplay between iron and lipid pathways throughout disease progression. Methods: We conducted a two-stage study design. In the discovery phase, proteomic profiling was performed in 5 GDM-PE patients and 10 GDM controls to identify critical hub proteins and dysregulated pathways. We then performed targeted validation in an independent first-trimester cohort consisting of 20 normal pregnant women, 14 GDM patients, and 6 GDM-PE patients. Levels of six key proteins: adiponectin, P-selectin, soluble transferrin receptor (sTFR), ferritin, fetuin-A, and apolipoprotein B, were measured using ELISA, and protein networks and clinical correlations were further analyzed. Results: Proteomic analysis identified 218 differentially expressed proteins in patients with GDM-PE, which were significantly enriched in the ferroptosis pathway; adiponectin and P-selectin were identified as key hub proteins. Targeted validation confirmed significant trends of increasing sTFR and decreasing fetuin-A across the disease continuum (P for trend < 0.05), suggesting a potential alteration in iron-lipid metabolic balance that may be related to ferroptosis-associated pathways. We observed progressive network rewiring: the physiological adiponectin-sTFR correlation was abolished in GDM, while a pathological fetuin-A-apolipoprotein B negative association emerged and intensified with disease severity, although not reaching statistical significance in the smaller subgroups. These molecular changes were mirrored in clinical associations: adiponectin correlated inversely with fasting glucose in GDM, whereas in GDM-PE, apolipoprotein B correlated strongly with 1-hour oral glucose tolerance test and the adiponectin-hemoglobin relationship reversed dramatically (r = -0.93, P = 0.008). Furthermore, logistic regression identified fetuin-A as an independent protective factor (adjusted odds ratio = 0.83, 95% CI: 0.65-0.96, P = 0.048) for GDM and sTFR as a risk factor (OR = 1.03, 95% CI: 1.01-1.06, P = 0.03) for disease severity. Conclusions: Our integrated analysis proposes a three-stage pathogenic model for GDM-PE, characterized by progressive lipid-iron axis dysregulation, which may be associated with ferroptosis-related processes but requires further validation. This network-based framework positions the core proteins of this axis as promising targets for early risk stratification.

Keywords: Pre-eclampsia, gestational diabetes, iron metabolism, ferroptosis, early diagnosis

Introduction

Gestational diabetes mellitus (GDM) and pre-eclampsia (PE) are highly prevalent and clinically significant pregnancy complications [1, 2], conferring substantial risks for adverse obstetric and neonatal outcomes as well as long-term maternal cardiometabolic disease and compromised offspring health [3-9]. PE, in particular, is a leading cause of fetal and maternal morbidity and mortality worldwide [10-12]. The co-occurrence of GDM and PE (GDM-PE) is not uncommon, with epidemiological studies reporting a prevalence ranging from 5.4‰ to 37.5‰ [5]. Indeed, GDM is a well-established risk factor for the subsequent development of PE [13] and they share several pathophysiological features, including oxidative stress, chronic inflammation, dyslipidemia, and endothelial dysfunction [14, 15]. Importantly, emerging evidence high-

https://doi.org/10.62347/SLAW4597

lights the role of iron metabolism dysregulation, and the involvement of such diverse systems points to a complex, multi-system pathological cross-talk [16-18]. This evidence supports the view of GDM-PE as a disorder arising from the interplay between metabolic and vascular dysfunction.

Accumulating evidence indicates a deleterious crosstalk between iron and lipid metabolism [19, 20]. Disrupted iron homeostasis promotes lipid accumulation through oxidative stress and mitochondrial dysfunction; these lipid abnormalities in turn exacerbate iron deposition and dysregulation, establishing a self-amplifying pathological loop [21, 22]. Ferroptosis, an iron-dependent form of regulated cell death, has been suggested to be involved in the pathophysiology of both GDM and PE, although direct clinical evidence remains limited [20, 23, 24]. Systemic iron availability, a critical prerequisite for ferroptosis, can be reliably assessed using ferritin, which reflects tissue iron stores, and soluble transferrin receptor (sTFR), which indicates cellular iron demand [25]. Elevated first-trimester ferritin is associated with GDM risk in a dose-dependent manner [26], and sTFR generally shows an inverse relationship with ferritin under physiological conditions. Among lipid markers, apolipoprotein B (apoB) is the core structural protein of all atherogenic lipoproteins [27] and is of particular relevance, as it directly quantifies the pool of atherogenic particles that drive endothelial dysfunction, a key feature of PE [28-31]. Moreover, apoB-containing lipoproteins serve as abundant substrates for lipid peroxidation, providing a direct mechanistic link between dyslipidemia and the execution of ferroptosis [32, 33].

We therefore hypothesize that fetuin-A may functionally connect these axes. This hepatokine acts as a potent inducer of systemic insulin resistance by inhibiting insulin receptor signaling and acting as an adaptor for TLR4-mediated inflammation [34]. Elevated fetuin-A is an independent risk factor for GDM [35], suggesting its role as a molecular hub linking dyslipidemia, inflammation, and insulin resistance. Thus, apolipoprotein B and iron metabolism represent critical nodes functionally connecting lipid metabolism to vascular injury and iron-dependent damage, thereby positioning the "lipid-iron metabolic axis" as a central hypothesis.

The convergence of these pathways underscores that GDM-PE is a complex, multi-system disorder whose pathogenic drivers are poorly defined. This complexity necessitates a systemic research approach. While mass spectrometry-based proteomics is powerful in biomarker discovery [36-38], its application to specifically profile GDM-PE against GDM alone remains limited. Therefore, fundamental questions remain: What distinct plasma protein alterations characterize the progression from GDM to GDM-PE, and can they serve as early predictive biomarkers?

We therefore performed a discovery-phase proteomic comparison of plasma from GDM-PE versus GDM patients to identify hub proteins and dysregulated pathways and validated the findings in an independent cohort, aiming to establish a protein fingerprint distinguishing GDM-PE from GDM, delineate its pathological features, and provide a basis for early risk stratification.

Materials and methods

Sample collection

The participants were pregnant women who took blood in the first trimester of pregnancy, including patients who had regular check-ups and without other complications. Shanghai Tenth People's Hospital separated the plasma immediately and stored it at -80°C between 2022 and 2023. Their antenatal care (in the first trimester) and postpartum care were followed longitudinally. Finally, 55 samples were collected, of which 15 samples were used for proteomics analysis and another 40 samples were used for ELISA validation. In plasma proteomics analysis set, 5 women developed GDM with PE and were used as the cases, while 10 women in GDM without PE were used as controls. In ELISA validate set, a total of 20 samples of GDM (N = 20) were used as the cases, including 6 GDM combined with PE (N = 6), 14 GDM without PE (N = 14), and 20 samples of normal control (N = 20).

A diagnosis of gestational diabetes was made based on recommendations from the International Association of Diabetes and Pregnancy Study Groups (IADPSG). During pregnancy between 24 and 28 weeks, screening and diagnosis of GDM are performed. The term GDM

refers to patients with fasting plasma glucose (FPG) levels that are more than 5.1 mmol/L (92 mg/dL) and/or 1 h plasma glucose >180 mg/dL or 2 h plasma glucose >153 mg/dL.

The International Society for the Study of Hypertension in Pregnancy (ISSHP) defines pre-eclampsia as new-onset gestational hypertension (systolic blood pressure ≥ 140 mm Hg and/or diastolic blood pressure ≥ 90 mm Hg) occurring at or after 20 weeks of gestation in conjunction with one or more of the following previously absent conditions: (1) Proteinuria (urine protein-to-creatinine ratio ≥ 30 mg/mmol [0.3 mg/mg]); (2) Other maternal organ dysfunction: acute kidney injury (serum creatinine ≥ 90 μmol/L [1 mg/dL]), hepatic involvement (alanine aminotransferase or aspartate aminotransferase > 40 IU/L) with or without right-upper-quadrant or epigastric pain; (3) Neurological complications (e.g., eclampsia, altered mental status, blindness, stroke, clonus, severe headache); (4) Hematological complications (platelet count < 150×10^3/μL, disseminated intravascular coagulation or hemolysis); (5) Uteroplacental dysfunction (fetal growth restriction, abnormal umbilical-artery Doppler waveforms or stillbirth).

Note, the simultaneous presence of gestational diabetes mellitus and pre-eclampsia (GDM-PE) must fulfill the diagnostic criteria for both disorders. Ethics committee approval was obtained for this study from Shanghai Tenth People's Hospital (Approval No. 25K131). All patients gave written informed consent before plasma (first trimester) was obtained for this study. Helsinki Declaration was followed in the study.

Plasma sample preparation

Blood samples were collected into an ethylene diamine tetraacetic acid (EDTA) tube containing an appropriate amount of anticoagulant. Then the tube was reversed repeatedly so that the anticoagulants and blood were fully mixed. Immediately, the blood was centrifuged at 4°C, with 3000 rpm, for 10 min. Finally, the plasma was stored at a temperature of -80°C in the refrigerator. After thawing at 4°C, 10 microliters of each sample were taken and added 190 microliters solution (50 mM TCEP + 140 mM 1% SDS) for disulfide bond reduction and alkylation. By using the Bradford method, the protein concentration was determined. After diluting the sample, an enzymatic hydrolysis solution was added (Trypsin, calcium chloride, TEAB). The dosage of trypsin was W (enzyme):W (substrate) = 1:50, and reacted overnight at 37°C for 16 hours. Using SPE Column C18 to bind the peptides, the supernatant was centrifuged at 4°C for 30 minutes, desalted by chromatography, and purified at 4°C with centrifuge. Freeze-dried peptides were stored at -20°C after being purified. As a quality control (QC) sample, all samples of the same volume were mixed and proceed with the same preprocessing method as the analysis samples. QC samples were run twice at the beginning of the test, and then every 5 samples were tested for QC samples.

Liquid chromatography-tandem mass spectrometry (LC-MS/MS) analysis

We diluted the sample concentration with Acetonitrile (ACN), removed impurities by filter membrane, and then put 1 ml of sample into a standard sample vial for a liquid chromatograph (EASY-nLC 1200, Thermo Fisher Scientific). In the chromatographic column of HypersilTM BDS C18, Mobile phase A was 0.1% Methanol, Mobile phase B was ACN, and flow rate was 1 ml/min for 90 minutes. Mass spectrometer parameters (Orbitrap ExplorisTM 480, Thermo Fisher Scientific). (1) MS: Resolution: 70,000; Auto Gain Control (AGC) target: 3e6; Maximum IT: auto; Scan Rates: 40 Hz at 200 m/z; Max Inject Time: 50 s. (2) dd-MS: Resolution: 35000; AGC target: 1e5; Max IT: 60 ms; TopN: 25; Fragmentation higher-energy collision dissociation (HCD): Normalized Collision Energy (NCE): 30; High-field asymmetric waveform ion mobility spectrometry (FAIMS) Pro Duo connects liquid chromatography and mass spectrometer, FAIMS CV range is 6-20 V, FAIMS Compensation Voltage (CV) step is 2 V.

Database search

Mascot Server (2.7) was used to process the raw MS data. Data independent acquisition (DIA) data was analyzed qualitatively by screening a minimum of two identified peptides with a parent mass tolerance of 10 ppm and a peptide false discovery rate (FDR) of 0.05. Further analysis was conducted utilizing Mascot output files including quantification.

Protein functional annotation and the enrichment analyses

GDM-PE and GDM sample data were subjected to differential expression analysis using R software's "limma" package. Log2 (fold change FC) > 0.26 proteins were set aside. The two-sided hypergeometric test was applied in this work to assess the enrichment analysis of the 218 differentially expressed proteins (DEPs). The ratio and *p* value were then determined with the hypergeometric distribution. The "pheatmap" and "ggplot2" packages were used to build DEP heat maps and volcano plots. Gene Ontology (GO) teams and Kyoto Encyclopedia of Genes and Genomes (KEGG) pathway functional enrichment studies were performed to look into the biological mechanisms of DEPs influencing GDM-PE. The Gene Ontology Consortium website (http://www.geneontology.org/) provided the GO annotation files on July 16, 2024, while the KEGG FTP server provided the KEGG annotation files on August 28, 2024.

We started by downloading the Gene Set Enrichment Analysis (GSEA) software (version 3.0) from the GSEA website (DOI: 10.1073/pnas.0506580102, http://software.broadinstitute.org/gsea/index.jsp) and the C2. Cp. Kegg. V7.4 Symbols from the Molecular Signatures Database (DOI: 10.1093/bioinformatics/btr260, http://www.gsea-msigdb.org/gsea/downloads.jsp). To evaluate the relevant pathways and biological mechanisms we separated them into GDM and GDM-PE groups based on the gene expression profile and phenotypic categorization. The Gene Set set the minimum gene count to 5 and the maximum gene count to 5000. It also set 1000 resampling, a *P* value < 0.05, and FDR < 0.25 as statistically significant. The KEGG pathway's final results were then shown.

Finally, we conducted GSEA for a single gene based on KEGG gene sets to investigate biomarkers' role. The samples were divided into two groups based on the median values of hub protein expression levels: the low expression group and the high expression group. A *p*-value of less than 0.05 was used for screening.

Weighted correlation network analysis (WGCNA)

A WGCNA analysis was used to identify significant modules in GDM-PE. Using the gene expression profile, we first estimated each gene's MAD (Median Absolute Deviation), deleted the top 50% of genes with the lowest MAD, eliminated outlier genes and samples via the R software package's "WGCNA" goodSamplesGenes method, and then applied WGCNA to create a scale-free co-expression network. The weighted adjacency matrix is created using the power function A_mn = |C_mn| ^ β (|C_mn| represents Pearson correlation between gene m and gene n; A_mn represents adjacency between gene m and gene n), after all paired genes have been calculated with the Pearson correlation matrix and average correlation method. A soft threshold parameter called β can highlight a strong gene association and penalize a weak one. Once the power of four has been chosen, the adjacency matrix is converted into a topological overlap matrix (TOM), which is used to calculate the corresponding dissimilarity (1-TOM) and measure the network connectivity of a gene. Network connectivity is defined as the sum of the adjacency matrix of the gene and all other genes assigned to the network gene. To identify genes with comparable expression patterns into gene modules, we perform average association hierarchical clustering using the TOM-based similarity measurement approach. Genes with similar expression profiles were grouped into different modules using dynamic tree cutting according to parameters of blockwiseModules, such as minModuleSize and mergeCutHeight. There were different colors for each module, with gray modules representing unassignable genes. Gene expression profiles for individual modules can be represented by first principal components called module eigengenes (ME). Phenotypes and modules were assessed using MEs. Further analysis was conducted on the module with the highest absolute correlation coefficient. A module membership (MM) is the correlation coefficient between a gene's expression value and a module's ME, indicating a gene's involvement in a module. The gene significance (GS) measures how genes and phenotypes are associated, based on the correlation coefficient between their expression values.

Identification of hub proteins

To obtain potential pathogenic gene sets associated with GDM-PE, we selected one of the modules, the most relevant to disease diagnosis, from WGCNA. The intersection of DEPs and

genes obtained by WGCNA was taken utilizing the "VennDiagram" package in R software. The String database (version 12.0; www.string-db.org) was used to create a protein-protein interaction (PPI) network to uncover connections between proteins. A minimum interaction score of 0.15 was set. Images downloaded from String were visualized by Cytoscape software, and significant interacting genes were found using a Molecular Complex Detection (MCODE) and Cytohubba plug-in. For further examination, all genes in the PPI network that could interact with one another were chosen.

Targeted validation

The six candidate proteins (adiponectin, P-selectin, ferritin, sTFR, apolipoprotein B, and fetuin-A) were quantified using commercial enzyme-linked immunosorbent assay (ELISA) kits (Cusabio Biotech Co., Ltd.) in an independent validation cohort (20 normal pregnancies, 14 GDM, 6 GDM-PE). All assays were performed in strict adherence to the manufacturer's protocols, with each sample measured in duplicate. Assay precision was confirmed by an intra-assay coefficient of variation of less than 5%.

Statistical analyses

The distribution of variables was examined to determine the appropriate statistical methods. Student t tests, Mann-Whitney U, Kruskal-Wallis or ANOVA tests were used to analyze differences between groups as appropriate. The chi-square test was used for comparison between groups. To examine the relationship between the variables, Pearson or Spearman correlation tests were employed. Univariate and multivariate logistic regression were constructed to determine the relationship between variables and outcomes. The discrimination of variables was quantified through receiver operating characteristic curves (ROC). The statistical analysis and sketching were conducted using R software (version 4.0.3), Cytoscape V3.9.1 and GraphPad Prism 8. All statistical tests were used in the two-sided variant, and *P* values less than 0.05 were considered statistically significant.

Results

Proteomics patient characteristics

We initially performed a discovery-based plasma proteomic analysis on ten patients with GDM alone (Group A) and five with GDM-PE (Group B), all of whom had no additional obstetric complications. Comparative analysis of clinical characteristics demonstrated that at the time of blood sampling, the GDM-PE group had significantly higher triglyceride (TG) levels compared to the GDM group ($P = 0.017$). Detailed clinical parameters of the two groups are summarized in **Table 1**. It should be noted that the discovery cohort included a relatively small number of GDM-PE cases ($n = 5$), which may limit statistical power and affect the stability of downstream clustering and differential expression analyses.

Plasma proteomic profiling

From 15 plasma samples (5 GDM-PE, 10 GDM), we identified 5,216 protein precursors, averaging 1,926 per sample (**Figure 1A**). Pearson's correlation coefficients between samples were high, indicating reproducible quantification (**Figure 1B**). Unsupervised principal component analysis (PCA) showed a general trend toward separation between GDM-PE and GDM groups; however, partial overlap was observed, with several GDM-PE samples clustering closer to the GDM group, likely reflecting biological heterogeneity and the limited sample size (**Figure 1C**); hierarchical clustering of all quantified proteins also grouped samples by disease status (**Figure 1D**). These distinct proteome profiles justified further differential expression analysis to identify key proteins underlying the group separation.

Differentially abundant proteins and functional annotation

Comparison between GDM-PE and GDM identified 218 differentially expressed proteins (DEPs, $|\log2FC| > 0.26$, $P < 0.05$), of which 160 were upregulated and 58 downregulated in GDM-PE. The volcano plot shows all 218 DEPs (**Figure 2A**); the heatmap displays the top twenty proteins (**Figure 2B**).

We performed enrichment analysis on the 218 DEPs using KEGG. KEGG analysis showed that the DEPs were enriched in pathways including NOD-like receptor signaling, complement and coagulation cascades, ferroptosis, biosynthesis of amino acids, citrate cycle (TCA cycle), and fatty acid metabolism (**Figure 2C**). GO analysis showed that the DEPs were enriched in biologi-

Table 1. Patient characteristics

	Overall, N = 15[1]	GDM, N = 10[1]	GDM-PE, N = 5[1]	Test statistic (Z)	*p*-value[2]
Age (years)	31.0 (29.8, 35.5)	32.0 (30.0, 36.2)	31.0 (29.7, 31.2)	-0.13	> 0.9
BMI (Kg/m^2)	23.4 (20.8, 26.6)	23.2 (20.4, 24.5)	26.3 (22.1, 27.0)	-0.67	0.5
MAP (mmHg)	84 (80, 89)	86 (84, 93)	80 (74, 81)	-2.27	0.023
CRP (mg/dL)	2.76 (1.57, 4.39)	2.58 (1.53, 3.73)	3.29 (2.76, 6.57)	-0.84	0.4
WBC (×10^9/L)	7.93 (7.04, 8.45)	8.28 (7.12, 8.46)	7.10 (7.08, 7.93)	-0.25	0.8
N (%)	74 (68, 76)	74 (72, 77)	66 (65, 76)	-0.67	0.5
L (%)	18.6 (15.4, 22.9)	18.1 (15.6, 19.8)	25.8 (15.5, 28.4)	-0.84	0.4
PLT (*10^9)	209 (166, 236)	206 (171, 235)	226 (161, 235)	-0.13	0.9
SOD (U/ml)	200 (196, 211)	209 (199, 217)	196 (195, 196)	-1.78	0.075
FBG (mmol/L)	4.20 (3.70, 4.75)	4.20 (3.70, 4.65)	4.10 (4.10, 4.80)	-0.25	0.8
1hPG (mmol/L)	9.40 (8.75, 10.10)	9.45 (8.83, 10.52)	8.80 (7.70, 9.60)	-1.04	0.3
2hPG (mmol/L)	8.90 (7.90, 9.40)	8.95 (8.12, 9.40)	8.90 (7.80, 9.00)	-0.13	0.9
TC (mmol/L)	4.62 (4.16, 5.10)	4.52 (4.13, 4.88)	5.45 (4.29, 5.51)	-1.04	0.3
TG (mmol/L)	1.79 (1.29, 2.20)	1.32 (1.26, 1.77)	2.21 (2.16, 2.98)	-2.39	0.017

[1]Median (IQR); n (%); [2]Wilcoxon rank sum test; Wilcoxon rank sum exact test; Fisher's exact test. Grade represents the severity grade of GDM-PE. According to gestational age, and The International Society for the Study of Hypertension in Pregnancy (ISSHP), PE was subclassified into early-onset preeclampsia (EOPE) (onset before 34 weeks) and LOPET (onset at or after 34 weeks). BMI, body mass index; MAP, mean arterial pressure; CRP, C-reactive protein; WBC, leucocyte count; L, lymphocyte; N, neutrophil; PLT, platelet; SOD, superoxide dismutase; FBG, fasting blood glucose; 1hPG, 1-hour postprandial blood glucose; 2hPG, 2-hour postprandial blood glucose; TG, triglyceride; TC, cholesterol.

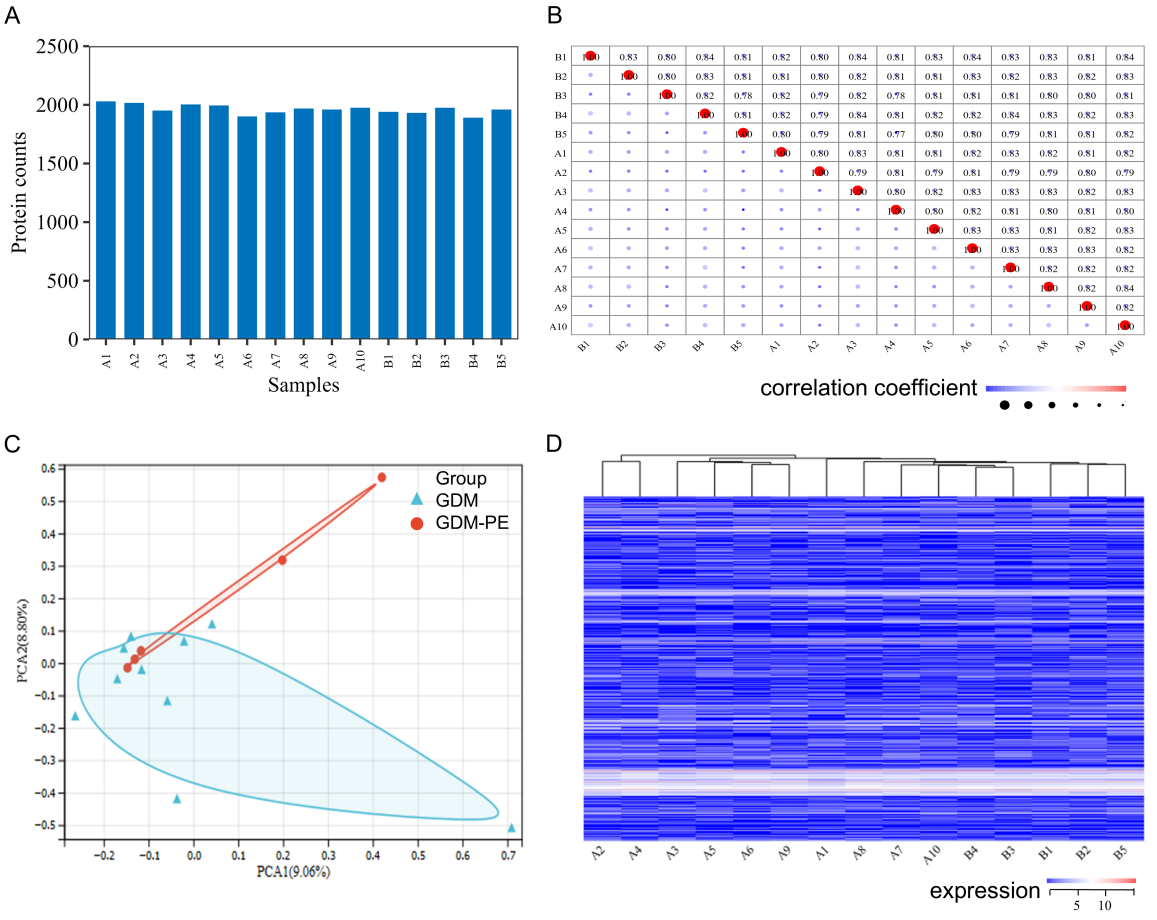

Figure 1. Quality control (QC) validation of Mass spectrometer (MS) data. A. Number distribution of every sample protein identified by mass spectrometry. B. Pearson's correlation of protein quantitation. C. Sample repeatability analysis by principal component analysis (PCA). D. The heatmap representation of abundance profile of all proteins in 2 groups.

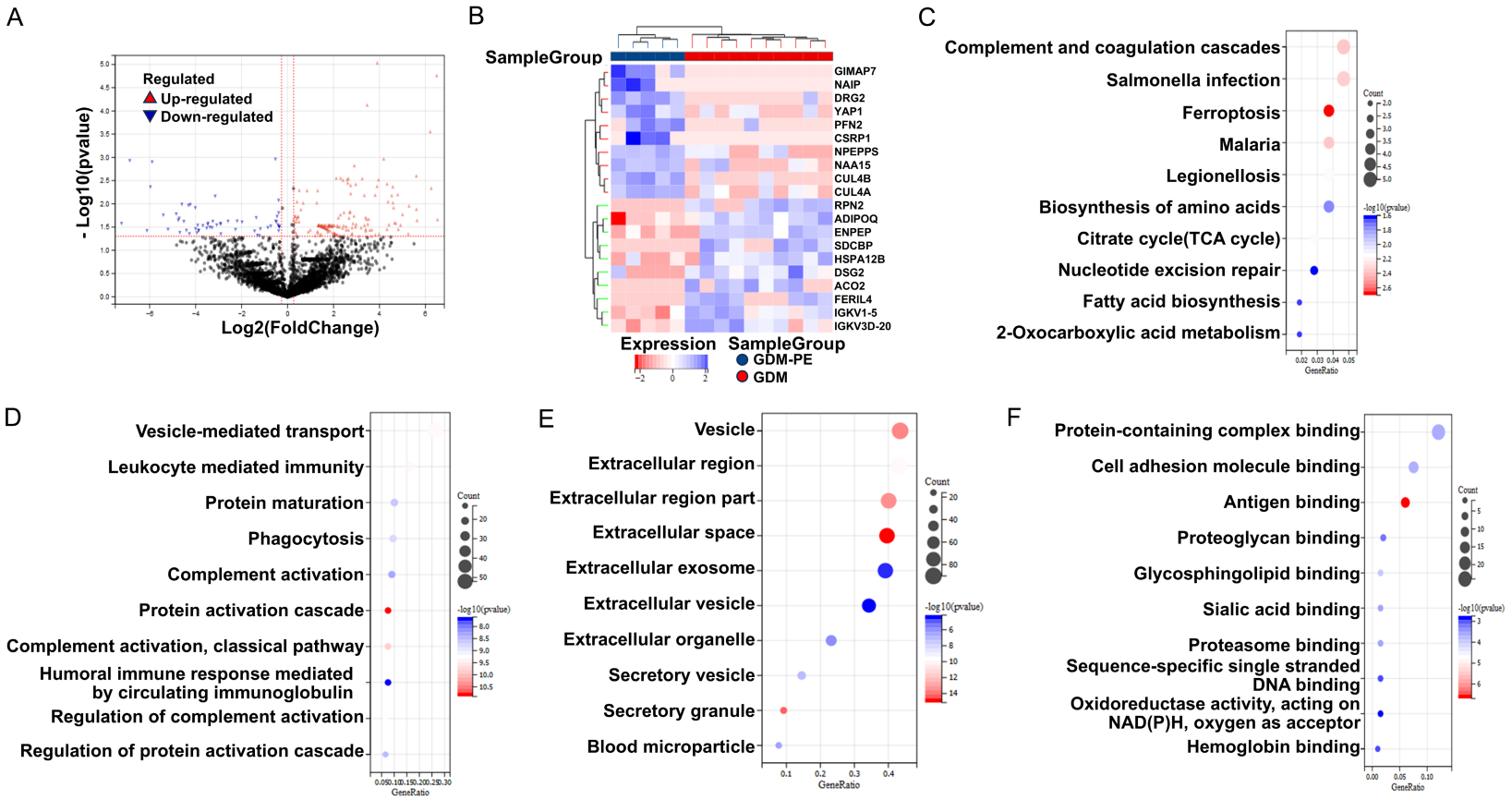

Figure 2. Differentially expressed proteins (DEPs) and functional annotation of differentially abundant proteins. (A) The volcano plot represents DEPs, of which the red and blue triangles refer to significant genes. (B) The heatmap shows the top 10 upregulated and downregulated DEPs, which are shown in red and blue colors. (C) Kyoto Encyclopedia of Genes and Genomes (KEGG) analysis of DEPs. (D-F) The DEP analysis includes biological process, cellular component and molecular function. In (C-F), y-axis represents KEGG pathways or Gene Ontology (GO) terms, and the x-axis represents gene ratio involved in corresponding pathways or terms. The size of circles represents gene numbers, and their color refers to *p*-value.

cal processes including vesicle-mediated transport, leukocyte-mediated immunity, phagocytosis, complement activation, and acute inflammatory response (**Figure 2D**). Cellular component enrichment included extracellular region, extracellular space, blood microparticle, and various vesicle-related components (**Figure 2E**). Molecular function analysis showed enrichment in cell adhesion molecule binding, antigen binding, glycolipid binding, and hemoglobin binding (**Figure 2F**).

We performed GSEA to complement the threshold-based DEP analysis. GDM-PE showed enrichment in carbohydrate metabolism and xenobiotics biodegradation pathways, including pentose and glucuronate interconversions and ascorbate and aldarate metabolism (**Figure 3**). In contrast, GDM showed greater enrichment in amino acid metabolism, particularly valine, leucine and isoleucine biosynthesis. Overall, GDM-PE displayed a profile linked to glucose metabolism and oxidative stress, whereas GDM showed alterations in branched-chain amino acid metabolism.

Construction of weighted co-expression network (WGCNA)

To identify biologically significant protein co-expression modules associated with GDM-PE, we performed a weighted gene co-expression network analysis (WGCNA). The analysis integrated the expression profiles of 5,216 proteins from the 15 samples in this study with proteomic data from an additional cohort of 10 pre-eclampsia (PE) patients and 10 healthy pregnant women, as previously published by our group [39]. This combined dataset enhanced the robustness of network construction.

A soft thresholding power of 4 was selected to achieve a scale-free topology (scale independence $R^2 = 0.89$; **Figure 4A**, **4B**), resulting in an average connectivity of 45.6. Using dynamic tree cutting with a minimum module size of 30 and a cut height of 0.25, we identified 36 distinct co-expression modules (**Figure 4C**). Among these, the black module demonstrated the strongest positive correlation with the GDM-PE phenotype ($r = 0.42$, $P = 0.01$; **Figure 4D**), and was therefore selected for further investigation. This module comprised 237 highly interconnected proteins. Module membership (MM) and gene significance (GS) analysis further confirmed a strong association between proteins within the black module and the disease phenotype ($r = 0.64$, $P = 5.3e\text{-}29$; **Figure 4E**).

Functional annotation of 28 overlapping hub proteins

To systematically investigate the core pathogenic pathways underlying GDM-PE, we intersected the 218 differentially expressed proteins (DEPs) with the key GDM-PE-related module (the black module, containing 237 proteins) identified by WGCNA, yielding 28 overlapping hub proteins (28 co-DEPs) (**Figure 5A**). These candidate proteins were subsequently subjected to KEGG pathway and Gene Ontology (GO) enrichment analyses.

KEGG enrichment analysis revealed that these hub proteins were significantly enriched in several metabolism and disease-related pathways, including “Malaria”, “AMPK signaling pathway”, “Selenocompound metabolism”, “RNA transport”, “One carbon pool by folate”, “Citrate cycle (TCA cycle)”, “Propanoate metabolism”, “Starch and sucrose metabolism”, “Proteasome”, and “Type II diabetes mellitus” (**Figure 5B**).

GO biological process (BP) analysis further indicated significant enrichment in key processes such as “low-density lipoprotein receptor particle metabolic process”, “oxoacid metabolic process”, “organic acid metabolic process”, “protein processing”, “platelet degranulation”, “protein maturation”, “tumor necrosis factor-mediated signaling pathway”, “Fc-epsilon receptor signaling pathway”, “regulation of protein metabolic process”, and “low-density lipoprotein particle clearance” (**Figure 5C**).

These enrichment results collectively suggest that metabolic reprogramming, particularly of glucose, lipid, and energy metabolism, alongside inflammatory immune activation and oxidative stress response may play central roles in the pathogenesis of GDM-PE, providing critical directions for understanding its molecular mechanisms.

Screening hub proteins by PPI networks

We examined 28 co-expressed proteins’ unique protein-protein interactions (PPIs), some of

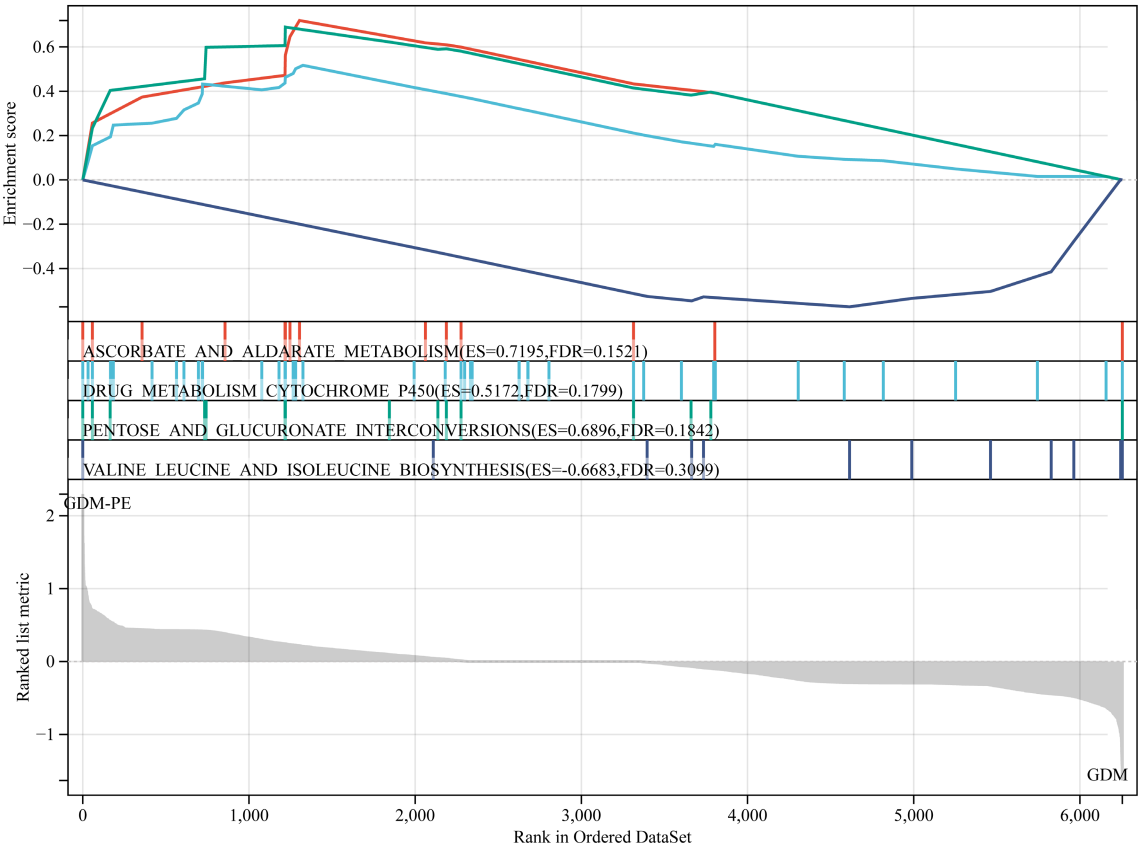

Figure 3. Gene set enrichment analysis (GSEA) of pathway enrichment in gestational diabetes mellitus pre-eclampsia (GDM-PE) versus GDM. Enrichment plots display representative pathways with corresponding normalized enrichment score (NES), nominal *p* value, and false discovery rate (FDR). Pathways with |NES| > 1, nominal P < 0.05, and FDR < 0.25 were considered significantly enriched. GDM-PE samples showed enrichment in pathways related to carbohydrate metabolism and oxidative stress, whereas GDM samples were enriched in amino acid metabolism pathways.

which were implicated in the PPI network's regulation (**Figure 6A**). Next, the network was analyzed using the CytoHubba plugin in Cytoscape with 12 topological algorithms (including MCC, DMNC, MNC, Degree, EPC, Bottleneck, EcCentricity, Closeness, Radiality, Betweenness, Stress, and Clustering Coefficient). The top 10 proteins from each algorithm were compiled, and three high-confidence hub proteins - P-selectin, PRELP, and adiponectin - were identified based on their consistent ranking across multiple methods (**Figure 6B**).

Furthermore, molecular complex detection using the MCODE plugin under stringent parameters (max. depth = 100, k-core = 2, degree cutoff = 2, node score cutoff = 0.2) identified one highly interconnected cluster containing P-selectin, CASP1, DUOX1, and adiponectin (**Figure 6C**). To elucidate the potential biological functions of this protein complex, we performed GO-BP enrichment analysis. The results revealed significant enrichment in terms strongly associated with inflammatory and stress-response pathways, including "inflammasome complex", "response to oxygen-containing compound", "positive regulation of response to stimulus", "cytokine-mediated signaling pathway", "response to lipid", "regulation of cellular component movement", "cellular response to cytokine stimulus", "response to organic substance", "response to stress", and "regulation of response to stress" (**Figure 6D**). These findings suggest that this protein cluster may be involved in inflammatory and oxidative stress responses in GDM-PE pathogenesis.

Targeted validation of bioinformatics hub proteins and ferroptosis pathway biomarkers

Validation cohort and protein selection: We validated six candidate proteins by ELISA in an

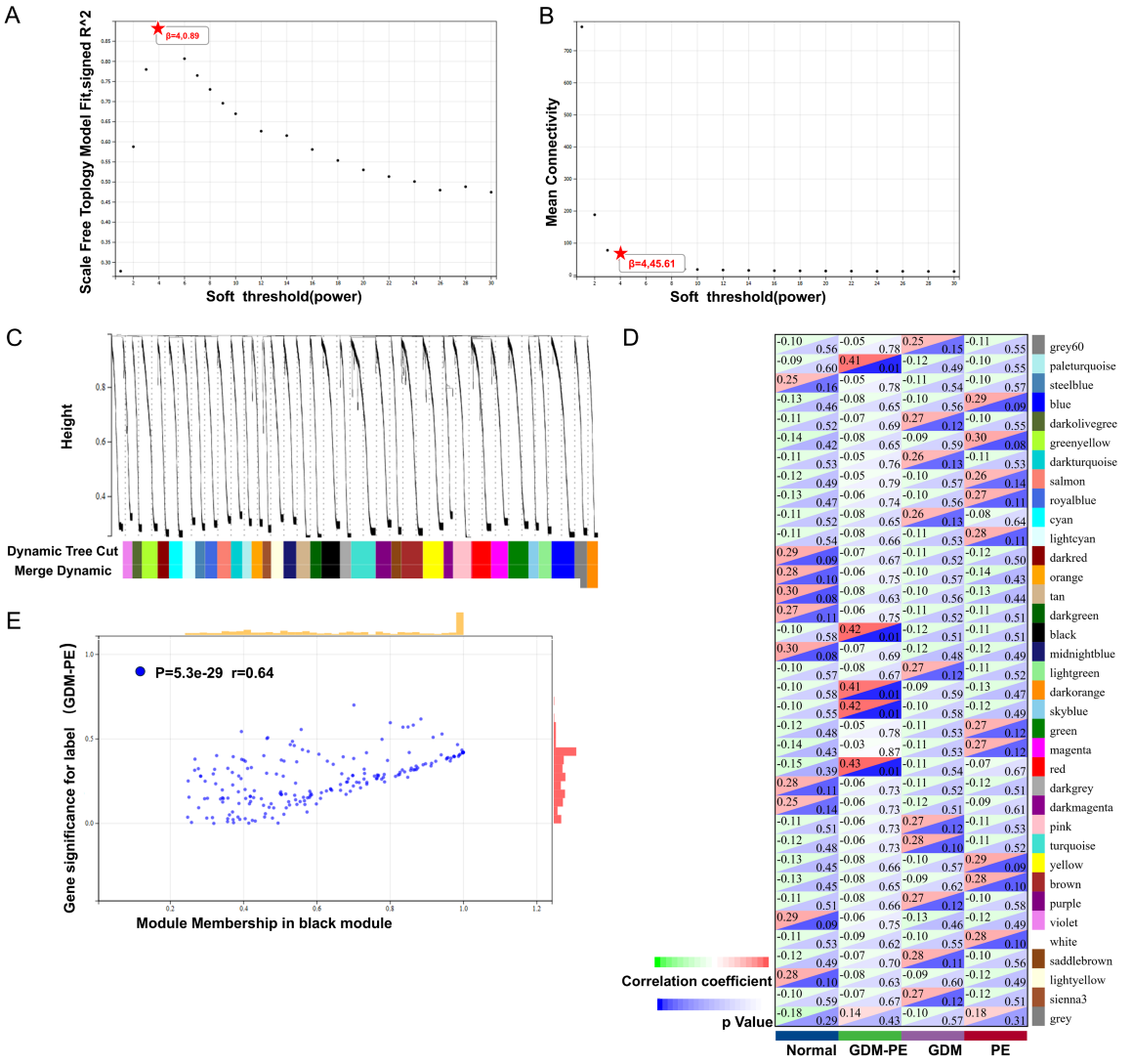

Figure 4. Weighted gene co-expression network analysis (WGCNA). A. Scale-free topology model fit index (R^2) as a function of soft-thresholding power, indicating optimal network construction ($R^2 \approx 0.89$ at power = 4). B. Mean connectivity across different soft-thresholding powers. C. Hierarchical clustering dendrogram of proteins showing module assignment. D. Heatmap of correlations between module eigengenes and clinical traits, with correlation coefficients (r) and corresponding *p* values displayed. E. Scatter plot showing the relationship between module membership (MM) and gene significance (GS) in the black module (r = 0.64, P = 5.3e-29).

independent first-trimester plasma cohort consisting of 20 normal pregnancies, 14 patients with uncomplicated GDM, and 6 patients with GDM-PE (**Table 2**). Including normal pregnancies allowed assessment of deviations from physiological homeostasis, and stratification of GDM patients (with or without PE) enabled evaluation of biomarker associations with disease severity. The proteins selected included: (1) Hub proteins from PPI analysis: adiponectin and P-selectin; (2) Core biomarkers of ferroptosis: soluble transferrin receptor (sTFR) and Ferritin; and (3) Functional regulators of insulin and lipid metabolism: fetuin-A and apolipoprotein B.

Alterations in protein levels and correlation network rewiring: Plasma profiling across the disease continuum from normal pregnancy to GDM and GDM-PE revealed significant trends of increasing sTFR and decreasing fetuin-A (P for trend < 0.05 for both). Post-hoc analysis confirmed that this dysregulation originated from significant differences between the GDM

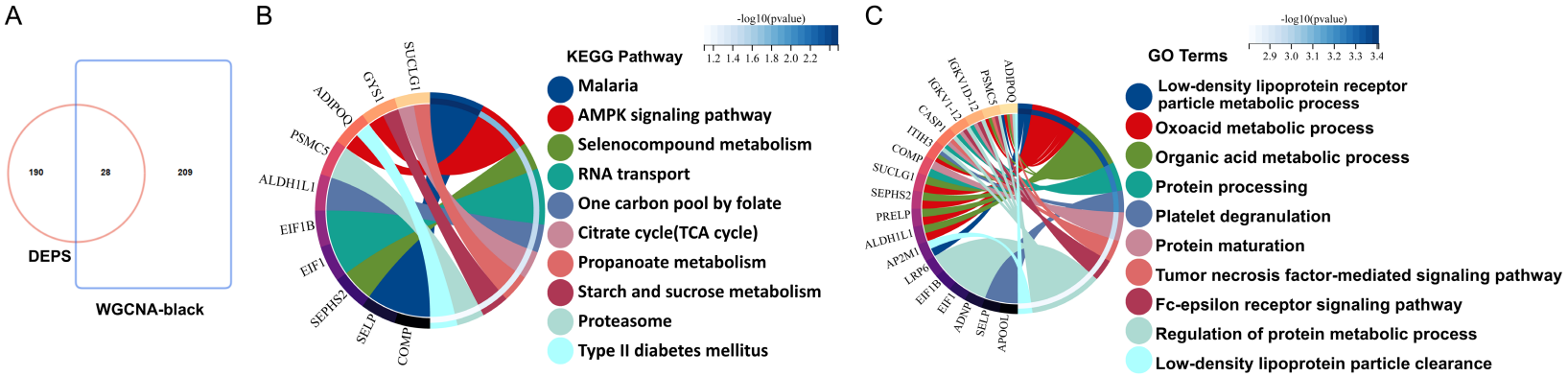

Figure 5. Functional annotation of 28 overlapping hub proteins. A. Venn diagram showing the intersection of DEGs via Limma and WGCNA-black module genes. B. KEGG enrichment analysis of 28 overlapping hub proteins. C. GO biological process (BP) analysis of 28 overlapping hub proteins.

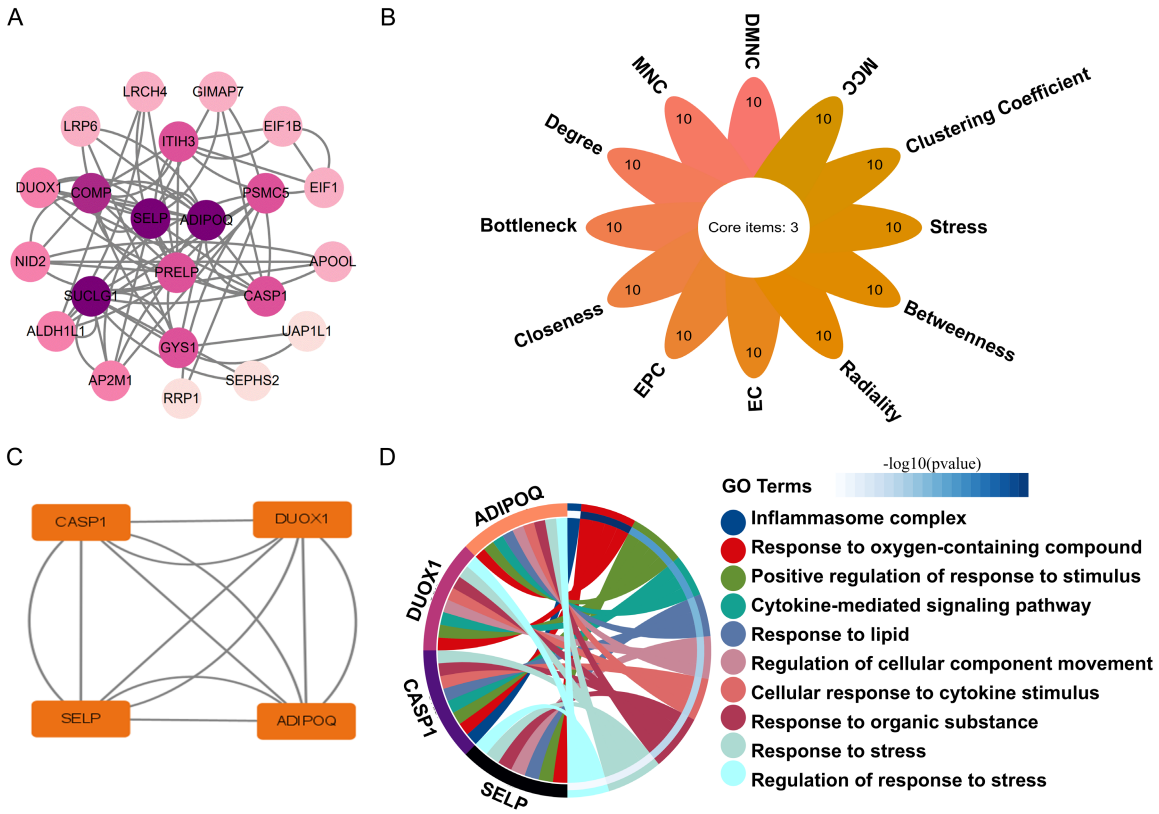

Figure 6. The recognition of node genes with the PPI network. A. Using the STRING database, total of 28 overlapping hub proteins were filtered into the PPI network and visualized by Cytoscape, the shade of the color represents the amount of degree. B. Flowergram showing the intersection of the top 10 proteins by 12 algorithms of the cytoHubba. C. The top one cluster PPI network in MCODE analysis. D. Enrichment analysis (GO-BP) of the top 1 MCODE genes function.

and normal groups (sTFR, P = 0.276; fetuin-A, P = 0.0493; **Figure 7A**, **7B**). The altered levels of both proteins were maintained in the GDM-PE subgroup, which showed no significant further change compared to the uncomplicated GDM group. In contrast, levels of ferritin, apolipoprotein B, adiponectin, and P-selectin did not differ significantly among the groups (**Figure 7C-F**).

Spearman correlation analysis across all 40 samples confirmed robust assay reliability, as seen in the strong negative correlation between ferritin and sTFR (r = -0.94, P < 0.001) (**Figure 8A**). Critically, we observed disease specific rewiring of correlation networks (**Figure 8B**, **8C**). A significant positive correlation between adiponectin and sTFR in normal pregnancies (r = 0.502, P = 0.026) was absent in the GDM group (r = 0.077, P = 0.748), indicating loss of physiological coordination. fetuin-A and apolipoprotein B were significantly negatively correlated in GDM patients (r = -0.555, P = 0.012), whereas no correlation was found in normal controls. P-selectin showed a notable negative correlation with apolipoprotein B in the full cohort (r = -0.348, P = 0.028). The correlation between P-selectin and fetuin-A shifted from significantly negative in normal pregnancies (r = -0.485, P = 0.032) to a positive trend in GDM (r = 0.355, P = 0.125), indicating a context-dependent relationship. The negative correlation between fetuin-A and apolipoprotein B progressively strengthened with increasing disease severity: r = 0.274 (P = 0.243) in normal pregnancies, r = -0.433 (P = 0.124) in GDM, and r = -0.657 (P = 0.175) in GDM-PE (**Figure 8D**). This pattern suggests a pathological interaction linked to disease stage.

Correlations with clinical parameters and predictive value

Candidate proteins versus clinical parameters: We assessed correlations between the six can-

Table 2. Clinical characteristics of validation patients

Group/Characteristic/No.	Overall N = 40[1]	GDM N = 20[1]	Normal N = 20[1]	Test statistic (Z)	*p*-value[2]
Age(years)	31.00 [29.00, 32.00]	31.50 [29.00, 32.50]	30.00 [29.00, 32.00]	-1.03	0.3
BMI (kg/m^2)	21.9 [20.2, 24.4]	24.0 [21.0, 26.8]	20.6 [19.5, 22.3]	-2.75	0.006
blood_pregnation[3]	11.42 ± 0.81	11.58 ± 0.72			0.56
In the first trimester					
Routine blood examination					
WBC (×10^9/L)	8.72 [7.18, 10.26]	9.41 [8.07, 11.84]	8.00 [6.92, 9.52]	-1.84	0.065
PLT (×10^9/L)	261 [217, 309]	282 [231, 321]	238 [211, 279]	-1.48	0.14
N (%)	74 [69, 77]	75 [69, 78]	71 [69, 76]	-1.28	0.2
Hb (g/L)	129 [118, 134]	134 [130, 138]	124 [116, 129]	-3.82	< 0.001
Anaemia				NA	> 0.9
Yes	2 (5.0%)	1 (5.0%)	1 (5.0%)		
No	38 (95%)	19 (95%)	19 (95%)		
Liver function					
ALT(U/L)	19 [11, 31]	21 [15, 33]	15 [8, 29]	-1.59	0.11
AST(U/L)	18 [13, 24]	20 [15, 24]	16 [12, 25]	-1.03	0.3
SOD	217 [200, 227]	216 [205, 227]	220 [197, 227]	-0.05	> 0.9
Renal function					
BUN (mmol/L)	2.60 [2.30, 3.20]	2.75 [2.40, 3.30]	2.50 [2.30, 3.00]	-1.03	0.3
Cr (μmol/L)	52.0 [48.0, 54.0]	51.5 [48.0, 54.0]	52.0 [49.0, 53.0]	-0.38	0.7
UA (μmol/L)	230 [194, 266]	231 [212, 265]	213 [188, 266]	-0.84	0.4
Coagulation function					
PT(s)	10.90 [10.50, 11.10]	10.85 [10.50, 11.10]	10.90 [10.40, 11.20]	-0.25	0.8
APTT(s)	26.40 [25.90, 28.60]	26.40 [26.05, 27.50]	26.40 [25.40, 28.90]	-0.25	0.8
D-Dimer (mg/L)	0.36 [0.24, 0.49]	0.40 [0.26, 0.48]	0.32 [0.24, 0.51]	-0.25	0.8
Fibrinogen (g/L)	3.74 [3.20, 4.36]	4.05 [3.35, 4.42]	3.64 [3.18, 4.28]	-0.84	0.4
FPG# (mmol/L)	4.90 [4.60, 5.30]	5.25 [4.70, 5.50]	4.70 [4.40, 4.90]	-2.60	0.009
Native				NA	0.222
Yes	13 (33%)	9 (45%)	4 (20%)		
No	27 (68%)	11 (55%)	16 (80%)		
Fatty liver				NA	0.028
Yes	9 (23%)	8 (40%)	1 (5.3%)		
No	30 (77%)	12 (60%)	18 (95%)		
Aspirin treatment				NA	0.056
Yes	5 (13%)	5 (25%)	0 (0%)		
No	35 (88%)	15 (75%)	20 (100%)		
Iron supply				NA	> 0.9
Yes	2 (5.0%)	1 (5.0%)	1 (5.0%)		
No	38 (95%)	19 (95%)	19 (95%)		
In the second trimester					
OGTT					
FPG (mmol/L)	4.28 [3.90, 4.62]	4.39 [4.00, 5.05]	3.98 [3.80, 4.40]	-2.60	0.036
1hPG (mmol/L)	8.80 [6.60, 11.10]	11.00 [9.35, 11.55]	6.60 [6.00, 7.60]	-4.12	< 0.001
2hPG (mmol/L)	7.00 [5.90, 9.00]	8.95 [7.85, 9.55]	6.20 [5.40, 6.60]	-4.05	< 0.001
In the third trimester					
Neonatal weight (g)	3,280 [2,990, 3,580]	3,195 [2,732, 3,460]	3,350 [3,180, 3,650]	-1.24	0.212
sBP (mmHg)	122 [115, 133]	130 [116, 143]	118 [115, 125]	-2.08	0.037
dBP (mmHg)	74 [71, 78]	76 [72, 88]	72 [70, 76]	-2.20	0.028
Insulin treatment				NA	0.5
Yes	2 (5.0%)	2 (10%)	0 (0%)		
No	38 (95%)	18 (90%)	20 (100%)		

Mode of delivery				NA	0.15
Vaginal delivery	15 (38%)	5 (25%)	10 (53%)		
Cesarean section	24 (62%)	15 (75%)	9 (47%)		
Neonatal gender				NA	0.6
Female	22 (56%)	10 (50%)	12 (63%)		
Male	17 (44%)	10 (50%)	7 (37%)		
ELISA					
P-selectin (ng/mL)	6,179 [5,255, 9,185]	6,242 [5,335, 8,928]	5,587 [5,248, 9,283]	-2.38	0.7
adiponectin (μg/mL)	30 [14, 47]	35 [17, 56]	23 [11, 36]	-1.28	0.2
fetuin-A (mg/L)	4.6 [2.2, 7.7]	3.5 [1.9, 6.1]	6.3 [3.6, 13.2]	-2.38	0.017
ferritin (ng/mL)	6 [3, 11]	4 [2, 10]	7 [3, 13]	-0.84	0.4
sTFR (ng/mL)	3 [1, 8]	6 [2, 10]	3 [1, 5]	-2.26	0.024
apolipoprotein B (g/L)	0.55 [0.31, 1.34]	0.54 [0.30, 1.31]	0.55 [0.32, 1.35]	-0.05	> 0.9

[1]Median [Q1, Q3]; n (%); NA, not applicable due to Fisher's exact test; [2]Wilcoxon rank sum test; Pearson's Chi-squared test; Wilcoxon rank sum exact test; NA; [3]mean ± sd. BMI, body mass index; WBC, leucocyte count; N, neutrophil; PLT, Platelet Count; SOD, superoxide dismutase; FPG, fasting plasma glucose; 1hPG, 1-hour postprandial blood glucose; 2hPG, 2-hour postprandial blood glucose; Hb, hemoglobin; PT, prothrombin time; APTT, activated partial thromboplastin time; sBP, systolic blood pressure; dBP, diastolic blood pressure; Native, local residency status; ALT, alanine aminotransferase; AST, aspartate aminotransferase; BUN, blood urea nitrogen; Cr, Creatinine; UA, uric acid.

didate proteins and clinical parameters using Spearman analysis. Analysis of the entire cohort (n = 40) revealed several significant associations. A positive correlation was observed between sTFR and hemoglobin (Hb) levels (r = 0.43, P = 0.007). Conversely, fetuin-A showed negative correlations with both 1-hour plasma glucose (1hPG) (r = -0.416, P = 0.009) and 2-hour plasma glucose (2hPG) (r = -0.327, P = 0.046) (**Figure 8A**). When stratified into normal pregnancy (n = 20) and GDM (n = 20) groups, distinct correlation patterns emerged. In the normal pregnancy group (**Figure 9A**), positive correlations were found between: fetuin-A and prothrombin time (PT) (r = 0.521, P = 0.019); ferritin and 1hPG (r = 0.445, P = 0.049); apolipoprotein B with both FPG (r = 0.492, P = 0.027) and creatinine levels (r = 0.506, P = 0.023); P-selectin and 2hPG (r = 0.490, P = 0.028). A negative correlation was observed between apolipoprotein B and activated partial thromboplastin time (APTT) (r = -0.477, P = 0.033). In the GDM group (**Figure 9B**), adiponectin showed negative correlations with: platelet count (r = -0.466, P = 0.038); FPG in first trimester (r = -0.515, P = 0.020); 1hPG (r = -0.603, P = 0.005). Positive correlations in the GDM group included, fetuin-A with blood urea nitrogen (r = 0.458, P = 0.042); P-selectin with PT (r = 0.502, P = 0.024); apoB with platelet count (r = 0.522, P = 0.018), but a negative correlation with blood urea nitrogen (r = -0.481, P = 0.032).

Further stratification into normal pregnancy (n = 20), uncomplicated GDM (n = 14), and GDM-PE (n = 6) groups revealed progressively changing correlation patterns.

The correlation between adiponectin and hemoglobin showed a dramatic shift from positive in normal pregnancies (r = 0.261, P = 0.221) to strongly negative in GDM-PE (r = -0.928, P = 0.008). Fetuin-A and fasting glucose correlation reversed from weak negative in normal pregnancies (r = -0.065, P = 0.740) to strongly positive in GDM-PE (r = 0.841, P = 0.036). Apolipoprotein B and 1hPG correlation strengthened from weak positive in normal (r = 0.198, P = 0.510) to strong positive in GDM-PE (r = 0.886, P = 0.033). Adiponectin correlated positively with uric acid (UA) in normal pregnancies (r = 0.128, P = 0.609), negatively in uncomplicated GDM (r = -0.563, P = 0.036), and positively again in GDM-PE (r = 0.086, P = 0.919) (**Figure 9C**).

These results demonstrate a dynamic rewiring of the relationships between core protein biomarkers and clinical parameters as pregnancy progresses from normal to GDM and further to GDM-PE.

Regression analysis and predictive value: Logistic regression was employed to assess the predictive value of fetuin-A and sTFR. After adjusting for first-trimester body mass index (BMI) and age, fetuin-A remained an independent protective factor against GDM (adjusted OR = 0.83, 95% CI: 0.65-0.96, P = 0.048), with an AUC of 0.723 (95% CI: 0.563-0.882) (**Figure 10**). In contrast, the significant univariate asso-

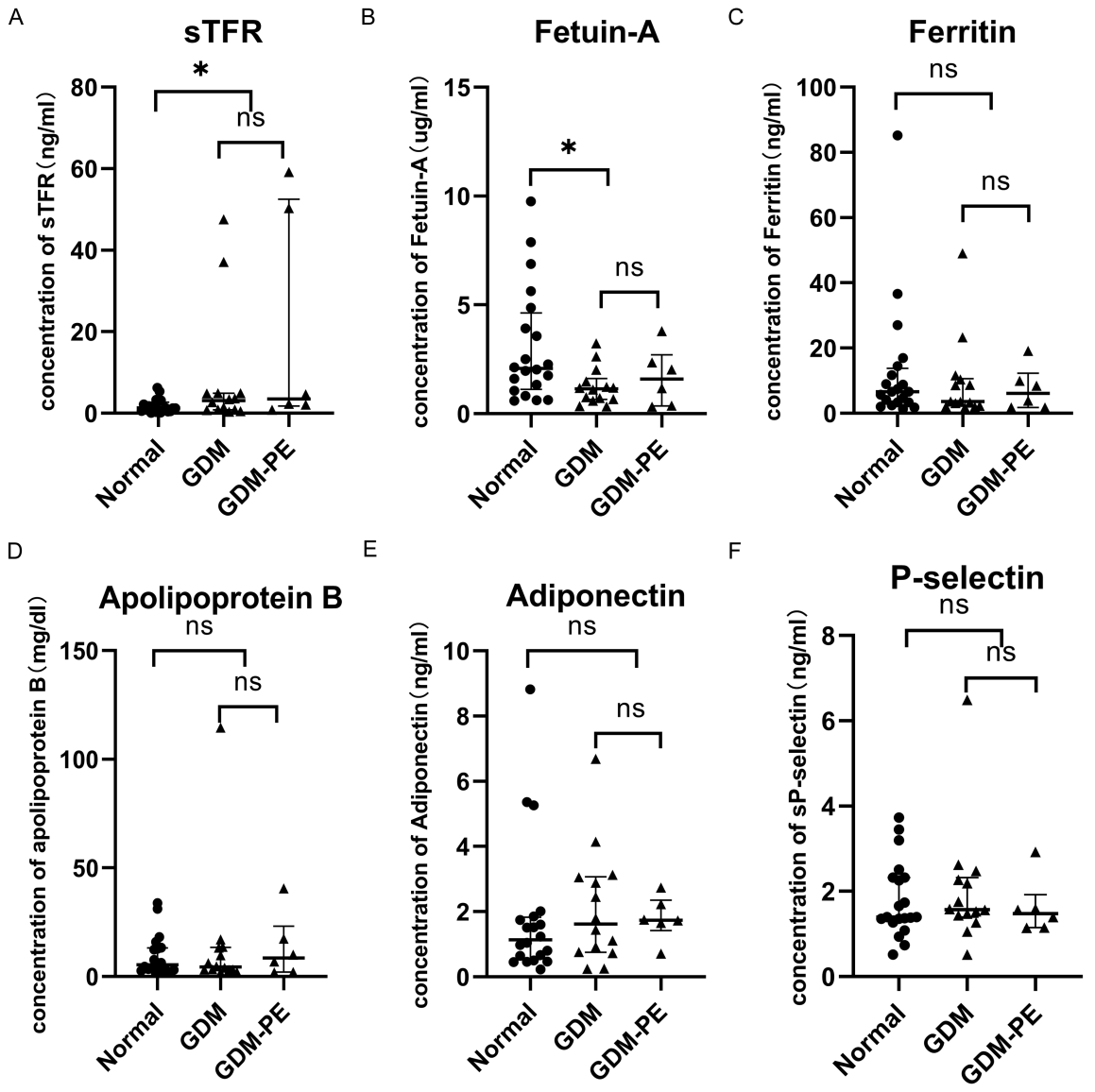

Figure 7. ELISA quantification of candidate proteins in individuals with and without gestational diabetes mellitus (GDM). A. Analysis results of soluble transferrin receptor (sTFR). B. Analysis results of fetuin-A. C. Analysis results of ferritin. D. Analysis results of apolipoprotein B. E. Analysis results of adiponectin. F. Analysis results of P-selectin. Data are presented as median and interquartile range (IQR). Group differences were analyzed using the Kruskal-Wallis test. *P < 0.05, **P < 0.01, ***P < 0.001; ns, not significant.

ciation between sTFR and disease severity (OR = 1.03, 95% CI: 1.01-1.06, P = 0.03) was abolished after multivariate adjustment (adjusted OR = 1.016, 95% CI: 0.988-1.050, P = 0.067), indicating that its effect is not independent of BMI. First-trimester BMI was itself the strongest independent predictor (adjusted OR = 1.542, 95% CI: 1.213-2.141, P = 0.022).

Discussion

Proteomic profiling of maternal plasma (from 5 GDM-PE vs. 10 GDM-only samples) effectively captured systemic metabolic and inflammatory perturbations. We identified 218 differentially expressed proteins (DEPs) in GDM-PE, which were significantly enriched in critical pathways, including the NOD-like receptor signaling pathway, complement and coagulation cascades, and ferroptosis, as revealed by KEGG analysis. This finding, corroborated by Gene Ontology (GO) and Gene Set Enrichment Analysis (GSEA), points to a profound dysregulation of inflammatory, metabolic, and oxidative stress responses in GDM-PE, suggesting the potential involve-

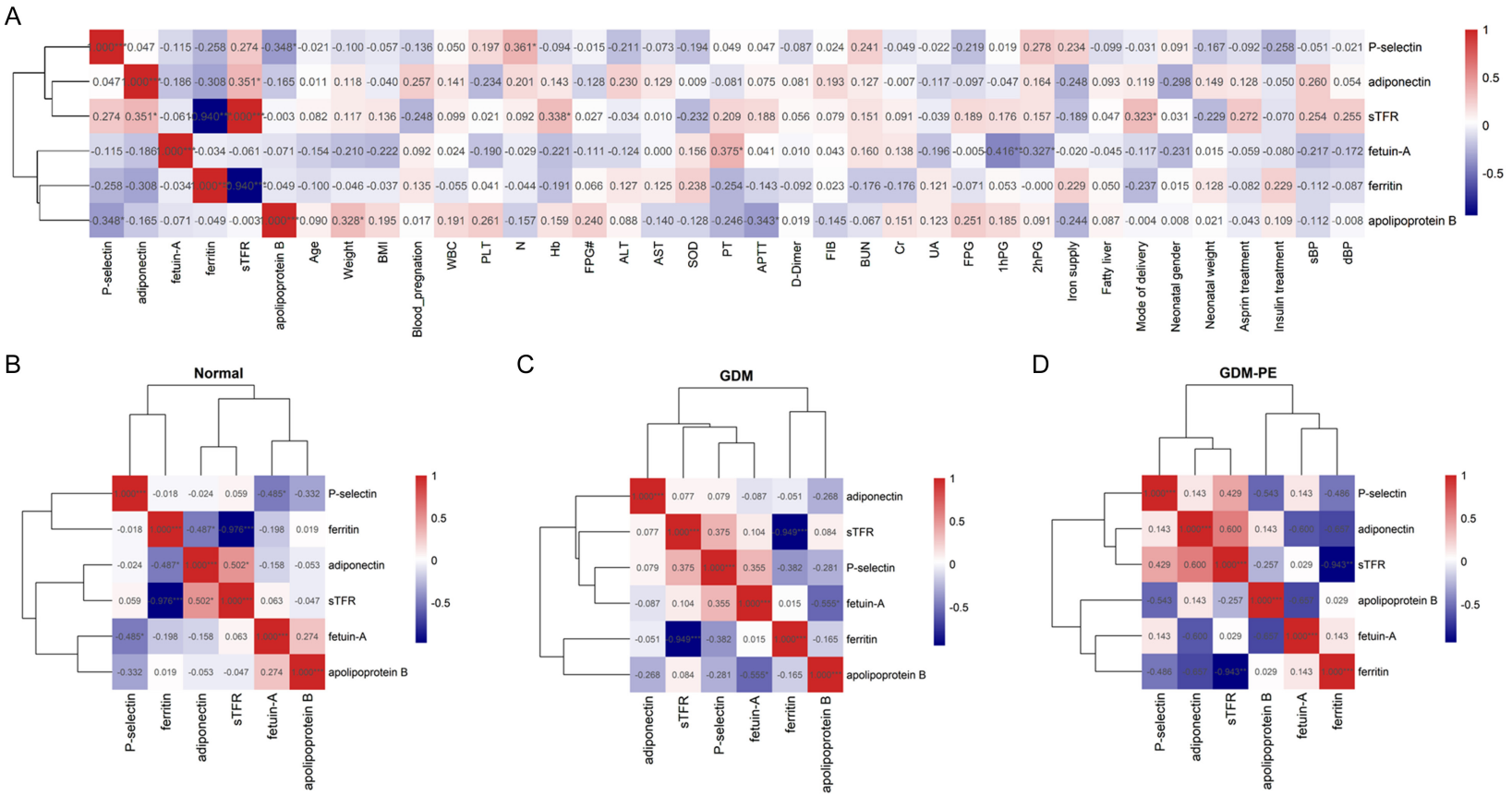

Figure 8. Spearman correlation analysis of candidate proteins. A. Correlation matrix across all samples (n = 40). B-D. Group-specific correlation matrices for normal pregnancy (n = 20), GDM (n = 20), and GDM-PE (n = 6), respectively. Color scale represents Spearman's correlation coefficient (ρ), ranging from negative (blue) to positive (red). Statistical significance is indicated as: *P < 0.05, **P < 0.01, ***P < 0.001.

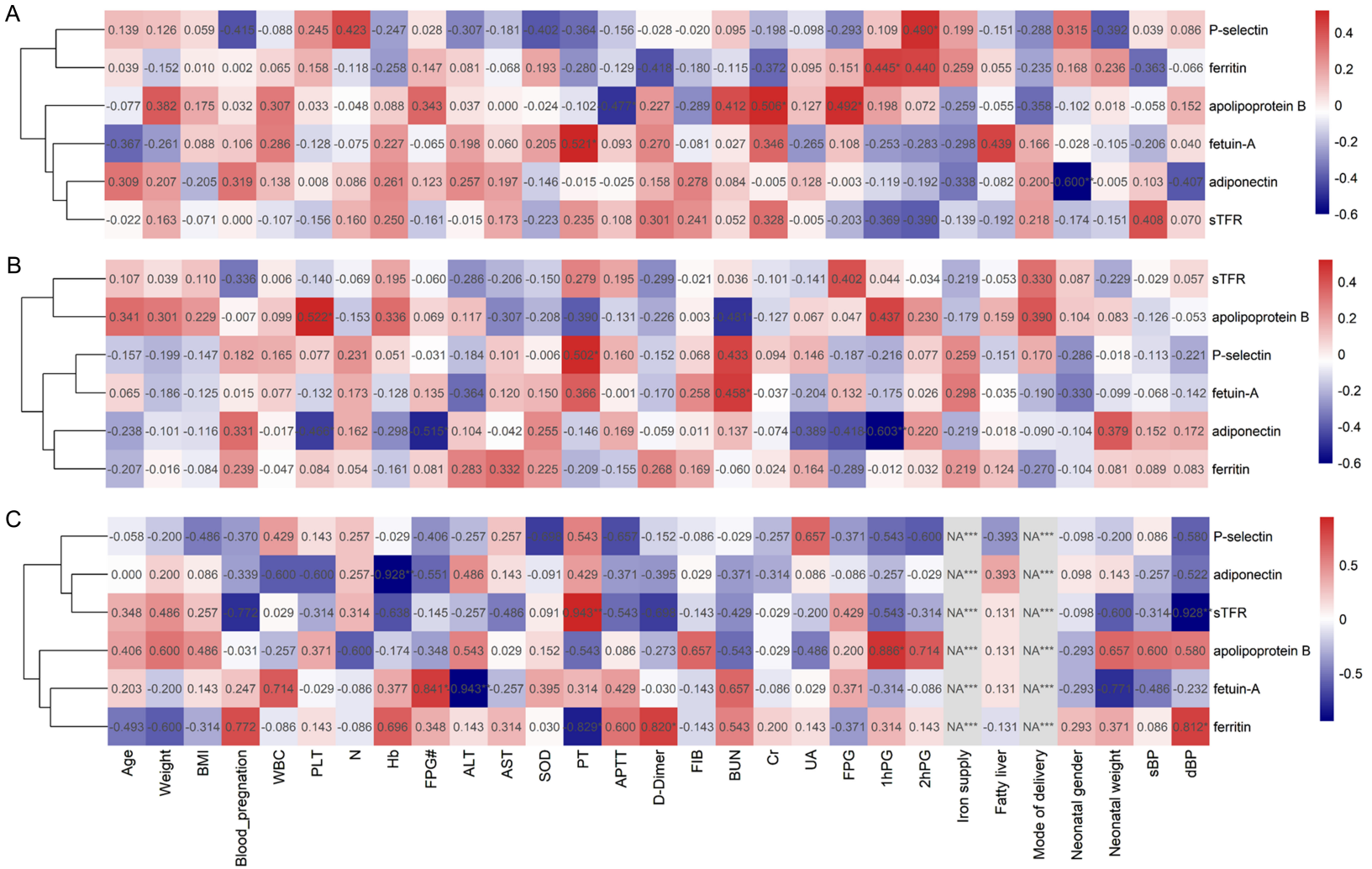

Figure 9. Correlations between core proteins and clinical parameters. A-C. Spearman correlation matrices for normal pregnancy (n = 20), GDM (n = 20), and GDM-PE (n = 6), respectively. Color scale represents Spearman's correlation coefficient (ρ), ranging from -1 (negative correlation) to +1 (positive correlation). Numerical values within each cell indicate correlation coefficients (ρ), and statistical significance is annotated as *P < 0.05, **P < 0.01, ***P < 0.001.

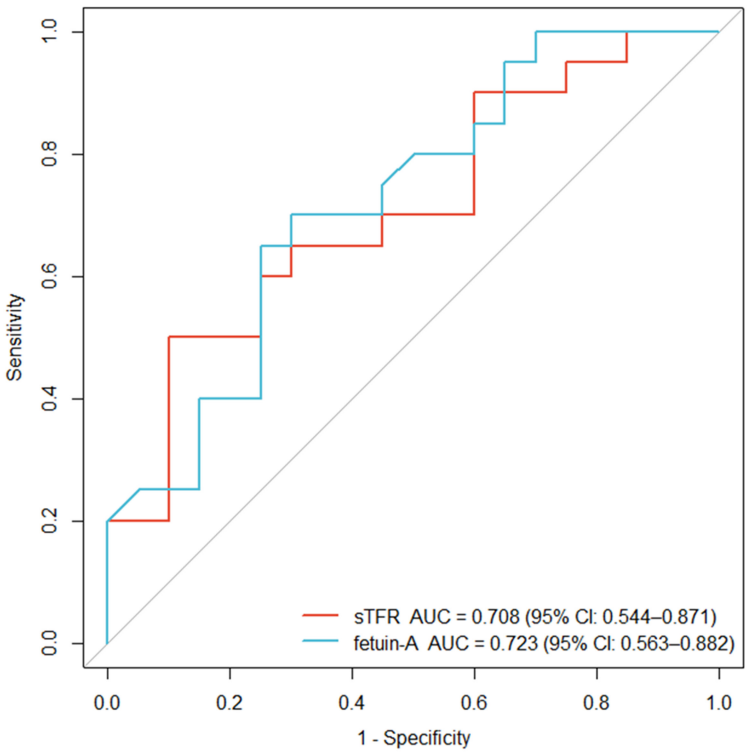

Figure 10. Receiver operating characteristic (ROC) curves evaluating the predictive performance of sTFR and fetuin-A for gestational diabetes mellitus (GDM). Area under the curve (AUC) values with corresponding 95% confidence intervals (CI) are shown. The optimal cut-off values were determined using the Youden index. Statistical significance of ROC analysis was assessed with $P < 0.05$.

ment of ferroptosis-related pathways [24], vascular dysfunction [40], and aberrant immune activation [41, 42] in its pathophysiology.

We intersected the 218 DEPs with the black module proteins (associated with the GDM-PE phenotype) from WGCNA and obtained 28 candidates. In the PPI network, multiple algorithms consistently ranked SELP and ADIPOQ as core functional nodes, pointing to their critical roles in the GDM-PE molecular network. The convergence of P-selectin (a key mediator of endothelial inflammation and coagulation [43, 44]) and adiponectin (a master regulator of metabolism [45]) as central hubs provides a compelling molecular rationale for the interplay between metabolic dysfunction and vascular pathology in GDM-PE. These discovery phase findings guided our selection of these targets for subsequent validation.

Our targeted validation delineates a disease associated dysregulation of the lipid-iron metabolic axis. This is first evidenced by a significant negative correlation between sTFR and ferritin ($r = -0.94$, $P < 0.001$), confirming assessment reliability. Most importantly, we identified significant monotonic trends of increasing sTFR and decreasing fetuin-A across the disease spectrum (Normal - > GDM - > GDM-PE). While post hoc analysis localized the primary shift to the transition from normal pregnancy to GDM, the GDM-PE subgroup maintained this dysregulated state. This supports a model wherein a functional iron deficiency [46, 47] and impaired fetuin-A signaling [48, 49] are established early and define a new, pathological steady state that characterizes the disease continuum. This altered iron-lipid metabolic state may be compatible with ferroptosis-related processes; however, this remains speculative in the absence of direct biomarker validation.

The role of fetuin-A in glucose metabolism was further corroborated by its significant negative correlations with 1hPG and 2hPG values in the entire cohort, aligning with its known insulin-sensitizing functions [50]. The observed decline in fetuin-A in GDM and its sustained low level in GDM-PE thus likely constitute a key persistent defect contributing to impaired glycemic control throughout the disease course.

We observed disease-specific loss of physiological correlations. The positive correlation between ADIPOQ and sTFR seen in normal pregnancies ($r = 0.502$, $P = 0.026$) disappeared in the GDM group, suggesting an early disruption of the physiological lipid-iron metabolic dialogue. ADIPOQ thus becomes a “functionally disconnected” regulator within this axis. Consistent with this, a negative correlation between ADIPOQ and fasting glucose appeared only in the GDM group ($r = -0.515$, $P = 0.020$), indicating that its insulin-sensitizing function is already impaired in early GDM [45, 51].

In the GDM-PE subgroup (n = 6), ADIPOQ showed a very strong negative correlation with hemoglobin (r = -0.93, P = 0.008). Despite the small sample size, this finding suggests that in severe disease, ADIPOQ dysfunction may extend beyond glucose metabolism, possibly reflecting a cross-talk disorder between the metabolic and hematopoietic systems. This could be related to systemic endothelial inflammation and oxidative stress, but further studies are needed. Beyond the loss of physiological correlations, new pathological associations emerged. Fetuin-A and ApoB showed no correlation in normal pregnancy but a significant negative correlation in GDM (r = -0.433), which strengthened with disease severity (r = -0.657 in the GDM-PE subgroup, n = 6). In parallel, fetuin-A showed a strong positive correlation with fasting glucose in GDM-PE (r = 0.84, P = 0.036). The magnitude of these changes suggests a mutually antagonistic relationship between the hepatoprotective fetuin-A and the pro-atherogenic ApoB, possibly reflecting hepatic dysfunction under metabolic stress. In the whole cohort, SELP showed a negative correlation with ApoB (r = -0.39, P = 0.016). This finding contrasts with the traditional view that both are pro-inflammatory factors and points to a unique compensatory mechanism in pregnancy.

We found that molecular changes were associated with alterations in clinical parameters, indicating early multi-system involvement. The GDM-specific correlation between ADIPOQ and fasting glucose reflected impaired insulin sensitizing function [52]. Positive correlations of ApoB with platelet count and negative correlations with creatinine linked an atherogenic environment to early coagulation and renal alterations, suggesting a potential increase in future cardiovascular risk [53]. In the GDM-PE subgroup (n = 6), ADIPOQ showed a strong negative correlation with hemoglobin (r = -0.93, P = 0.008). This observation indicates a possible disruption of crosstalk between the metabolic and hematopoietic systems in advanced disease, which may be related to systemic endothelial inflammation and oxidative stress [54, 55].

Our data suggest a progression from initial dysfunction to systemic collapse. In GDM, the first observable alteration is a breakdown of homeostatic interactions, exemplified by the loss of correlation between ADIPOQ and sTFR. During this stage, aberrant associations also begin to emerge, such as the negative correlation between fetuin-A and ApoB (r = -0.433). As the disease advances to GDM-PE, these aberrant interactions become more pronounced (r = -0.657), and the failure of the molecular network becomes fully manifested through extreme clinical phenotypes, ultimately leading to multisystem dysfunction.

Logistic regression showed that fetuin-A was an independent protective factor for GDM (adjusted OR = 0.83, 95% CI: 0.65-0.96, P = 0.048). In contrast, the univariate association between sTFR and disease severity (OR = 1.03, P = 0.03) lost significance after adjustment for BMI (adjusted OR = 1.016, P = 0.067), suggesting that its effect is largely attributable to adiposity. These results indicate an interdependence among iron regulation, adiposity, and inflammation. Together with the correlation shifts observed between fetuin-A, sTFR, and other proteins, the data support a dynamic process: disruption of iron metabolism begins with a decrease in fetuin-A (early GDM risk), followed by changes in sTFR that parallel metabolic deterioration, and is largely driven by adiposity.

We identified a dysregulated lipid-iron metabolic axis from the six core proteins involved in iron metabolism, lipid regulation, and inflammation. The disease-specific correlation patterns and network alterations among these proteins, detected in an independent first-trimester cohort and supported by correlations with clinical parameters, provide an integrated view of GDM-PE pathogenesis. The disease-specific correlation patterns and network rewiring among these proteins, validated in an independent first-trimester cohort and supported by their correlations with key clinical parameters, provide a novel integrative perspective on the pathogenesis of GDM-PE. Our findings support a progressive model wherein the disease evolves through a systematic rewiring of molecular networks, from an initial disconnection of physiological pathways to adversarial rewiring and ultimately to external multi-system collapse. These proteins may contribute to early pathological processes and hold promise as predictive biomarkers for early risk stratification and targeted preventive strategies.

Several limitations should be considered when interpreting our findings. First, the sample size of the discovery proteomics cohort, particularly the GDM-PE subgroup, was limited. This may affect the robustness of PCA clustering and the identification of differentially expressed proteins. Therefore, the proteomics findings should be regarded as exploratory and hypothesis-generating rather than definitive. Thus, we partially mitigated this limitation by performing targeted validation in an independent cohort, which provided additional support for the observed trends in key candidate proteins. Second, this study did not include direct measurements of ferroptosis-related biomarkers, such as lipid peroxidation products, antioxidant enzymes, or iron ion levels. Therefore, the involvement of ferroptosis in GDM-PE cannot be directly confirmed and should be interpreted as a hypothesis generated from pathway enrichment analysis rather than a demonstrated mechanism.

Conclusions

According to bioinformatics analyses, GDM-PE patients lack key hematological functional regulation. By screening potential biomarkers of GDM-PE and developing a nomogram to complement existing clinical parameters in diagnosing and predicting risk, our findings provide a proteomics-based characterization of lipid-iron metabolic alterations and identify candidate biomarkers for early risk stratification of GDM-PE. Early detection of high-risk pregnancies may be facilitated by identifying maternal factors that may assist in predicting the outcome and facilitating close follow-up and prevention of pregnancy complications. There is important acknowledgement that no single biomarker is likely to be effective as a sensitive, specific, or robust test, and that risk prediction algorithms may require a combination of biomarkers and maternal risk factors. However, the primary contribution of this study lies in the identification of candidate biomarkers and network alterations associated with disease progression, rather than in establishing a definitive mechanistic role for ferroptosis. Further studies incorporating direct ferroptosis-related biomarker measurements are required to validate the mechanistic implications suggested by this study.

Disclosure of conflict of interest

None.

Address correspondence to: Zhongping Cheng, Department of Obstetrics and Gynecology, Shanghai Tenth People's Hospital, School of Clinical Medicine of Nanjing Medical University, No. 301, Middle Yanchang Road, Jing'an District, Shanghai 200072, China. Tel: +86-021-66307151; Fax: +86-021-64307151; E-mail: 1701580@tongji.edu.cn

References

[1] Wu P, Green M and Myers JE. Hypertensive disorders of pregnancy. BMJ 2023; 381: e071653.

[2] Sweeting A, Hannah W, Backman H, Catalano P, Feghali M, Herman WH, Hivert MF, Immanuel J, Meek C, Oppermann ML, Nolan CJ, Ram U, Schmidt MI, Simmons D, Chivese T and Benhalima K. Epidemiology and management of gestational diabetes. Lancet 2024; 404: 175-192.

[3] Ramlakhan KP, Johnson MR and Roos-Hesselink JW. Pregnancy and cardiovascular disease. Nat Rev Cardiol 2020; 17: 718-731.

[4] Hinkle SN, Schisterman EF, Liu D, Pollack AZ, Yeung EH, Mumford SL, Grantz KL, Qiao Y, Perkins NJ, Mills JL, Mendola P and Zhang C. Pregnancy complications and long-term mortality in a diverse cohort. Circulation 2023; 147: 1014-1025.

[5] Jiang L, Tang K, Magee LA, von Dadelszen P, Ekeroma A, Li X, Zhang E and Bhutta ZA. A global view of hypertensive disorders and diabetes mellitus during pregnancy. Nat Rev Endocrinol 2022; 18: 760-775.

[6] Friis T, Bergman L, Hesselman S, Lindström L, Junus K, Cluver C, Escudero C and Wikström AK. Gestational hypertension, preeclampsia, and eclampsia and future neurological disorders. JAMA Neurol 2025; 82: 142-151.

[7] Chen A, Tan B, Du R, Chong YS, Zhang C, Koh AS and Li LJ. Gestational diabetes mellitus and development of intergenerational overall and subtypes of cardiovascular diseases: a systematic review and meta-analysis. Cardiovasc Diabetol 2024; 23: 320.

[8] Gu Y, Lu J, Li W, Liu H, Wang L, Leng J, Li W, Zhang S, Wang S, Tuomilehto J, Yu Z, Yang X, Baccarelli AA, Hou L and Hu G. Joint associations of maternal gestational diabetes and hypertensive disorders of pregnancy with overweight in offspring. Front Endocrinol (Lausanne) 2019; 10: 645.

[9] Lin YW, Lin MH, Pai LW, Fang JW, Mou CH, Sung FC and Tzeng YL. Population-based study

on birth outcomes among women with hypertensive disorders of pregnancy and gestational diabetes mellitus. Sci Rep 2021; 11: 17391.
[10] Sliwa K and Boehm M. Incidence and prevalence of pregnancy-related heart disease. Cardiovasc Res 2014; 101: 554-560.
[11] Hettiarachchi A, Jayaratne K, De Silva C, Senanayake H, Lokunarangoda N and Agampodi S. Heart disease complicating pregnancy as a leading cause of maternal deaths in LMIC settings: the Sri Lankan experience. Lancet Reg Health Southeast Asia 2023; 15: 100223.
[12] Musarandega R, Nyakura M, Machekano R, Pattinson R and Munjanja SP. Causes of maternal mortality in Sub-Saharan Africa: a systematic review of studies published from 2015 to 2020. J Glob Health 2021; 11: 04048.
[13] Venkatesh KK, Lynch CD, Powe CE, Costantine MM, Thung SF, Gabbe SG, Grobman WA and Landon MB. Risk of adverse pregnancy outcomes among pregnant individuals with gestational diabetes by race and ethnicity in the United States, 2014-2020. JAMA 2022; 327: 1356-1367.
[14] Chappell LC, Cluver CA, Kingdom J and Tong S. Pre-eclampsia. Lancet 2021; 398: 341-354.
[15] Hivert MF, Backman H, Benhalima K, Catalano P, Desoye G, Immanuel J, McKinlay CJD, Meek CL, Nolan CJ, Ram U, Sweeting A, Simmons D and Jawerbaum A. Pathophysiology from preconception, during pregnancy, and beyond. Lancet 2024; 404: 158-174.
[16] Gumilar KE, Priangga B, Lu CH, Dachlan EG and Tan M. Iron metabolism and ferroptosis: a pathway for understanding preeclampsia. Biomed Pharmacother 2023; 167: 115565.
[17] Xu Q, Zhu C, Li L, Li J, An Z and Tang C. The role of ferroptosis in women's health and diseases. MedComm (2020) 2025; 6: e70296.
[18] Rawal S, Hinkle SN, Bao W, Zhu Y, Grewal J, Albert PS, Weir NL, Tsai MY and Zhang C. A longitudinal study of iron status during pregnancy and the risk of gestational diabetes: findings from a prospective, multiracial cohort. Diabetologia 2017; 60: 249-257.
[19] Dixon SJ and Olzmann JA. The cell biology of ferroptosis. Nat Rev Mol Cell Biol 2024; 25: 424-442.
[20] Liu M, Wu K and Wu Y. The emerging role of ferroptosis in female reproductive disorders. Biomed Pharmacother 2023; 166: 115415.
[21] Rockfield S, Chhabra R, Robertson M, Rehman N, Bisht R and Nanjundan M. Links between iron and lipids: implications in some major human diseases. Pharmaceuticals (Basel) 2018; 11: 113.
[22] Eid R, Arab NT and Greenwood MT. Iron mediated toxicity and programmed cell death: a review and a re-examination of existing paradigms. Biochim Biophys Acta Mol Cell Res 2017; 1864: 399-430.
[23] Xie X, Liu J, Gao J, Shang C, Jiang Y, Chen L, Qian Z, Liu L, Wu D, Zhang Y, Ru Z and Zhang Y. The crosstalk between cell death and pregnancy related diseases: a narrative review. Biomed Pharmacother 2024; 176: 116815.
[24] Zhang Y, Lu Y and Jin L. Iron metabolism and ferroptosis in physiological and pathological pregnancy. Int J Mol Sci 2022; 23: 9395.
[25] Harms K and Kaiser T. Beyond soluble transferrin receptor: old challenges and new horizons. Best Pract Res Clin Endocrinol Metab 2015; 29: 799-810.
[26] Zhang X, Wu M, Zhong C, Huang L, Zhang Y, Chen R, Zhou X, Xu S, Li Q, Cui W, Wang X, Chen X, Lin L, Zhang G, Xiong G, Sun G, Yang X, Hao L, Jin Z and Yang N. Association between maternal plasma ferritin concentration, iron supplement use, and the risk of gestational diabetes: a prospective cohort study. Am J Clin Nutr 2021; 114: 1100-1106.
[27] Sniderman AD, Dufresne L, Pencina KM, Bilgic S, Thanassoulis G and Pencina MJ. Discordance among apoB, non-high-density lipoprotein cholesterol, and triglycerides: implications for cardiovascular prevention. Eur Heart J 2024; 45: 2410-2418.
[28] van Zwol W, van de Sluis B, Ginsberg HN and Kuivenhoven JA. VLDL biogenesis and secretion: it takes a village. Circ Res 2024; 134: 226-244.
[29] Marston NA, Giugliano RP, Melloni GEM, Park JG, Morrill V, Blazing MA, Ference B, Stein E, Stroes ES, Braunwald E, Ellinor PT, Lubitz SA, Ruff CT and Sabatine MS. Association of apolipoprotein b-containing lipoproteins and risk of myocardial infarction in individuals with and without atherosclerosis: distinguishing between particle concentration, type, and content. JAMA Cardiol 2022; 7: 250-256.
[30] Richardson TG, Wang Q, Sanderson E, Mahajan A, McCarthy MI, Frayling TM, Ala-Korpela M, Sniderman A, Smith GD and Holmes MV. Effects of apolipoprotein B on lifespan and risks of major diseases including type 2 diabetes: a mendelian randomisation analysis using outcomes in first-degree relatives. Lancet Healthy Longev 2021; 2: e317-e326.
[31] Borén J, Taskinen MR and Packard CJ. Biosynthesis and metabolism of ApoB-containing lipoproteins. Annu Rev Nutr 2024; 44: 179-204.
[32] Negre-Salvayre A, Swiader A, Salvayre R and Guerby P. Oxidative stress, lipid peroxidation and premature placental senescence in preeclampsia. Arch Biochem Biophys 2022; 730: 109416.
[33] Leong XF. Lipid oxidation products on inflammation-mediated hypertension and athero-

sclerosis: a mini review. Front Nutr 2021; 8: 717740.
[34] Pal D, Dasgupta S, Kundu R, Maitra S, Das G, Mukhopadhyay S, Ray S, Majumdar SS and Bhattacharya S. Fetuin-A acts as an endogenous ligand of TLR4 to promote lipid-induced insulin resistance. Nat Med 2012; 18: 1279-1285.
[35] Jin C, Lin L, Han N, Zhao Z, Liu Z, Luo S, Xu X, Liu J and Wang H. Effects of dynamic change in fetuin-A levels from the first to the second trimester on insulin resistance and gestational diabetes mellitus: a nested case-control study. BMJ Open Diabetes Res Care 2020; 8: e000802.
[36] Roverso M, Dogra R, Visentin S, Pettenuzzo S, Cappellin L, Pastore P and Bogialli S. Mass spectrometry-based "omics" technologies for the study of gestational diabetes and the discovery of new biomarkers. Mass Spectrom Rev 2023; 42: 1424-1461.
[37] Navajas R, Corrales F and Paradela A. Quantitative proteomics-based analyses performed on pre-eclampsia samples in the 2004-2020 period: a systematic review. Clin Proteomics 2021; 18: 6.
[38] Lapolla A and Traldi P. Proteomic approaches in the study of placenta of pregnancy complicated by gestational diabetes mellitus. Biomedicines 2022; 10: 2272.
[39] Xie Y, Zhou W, Tao X, Lv H and Cheng Z. Early gestational blood markers to predict pre-eclampsia complicating gestational diabetes mellitus. Diabetes Metab Syndr Obes 2023; 16: 1493-1503.
[40] Hu XQ and Zhang L. Oxidative regulation of vascular Ca(v)1.2 channels triggers vascular dysfunction in hypertension-related disorders. Antioxidants (Basel) 2022; 11: 2432.
[41] Jung E, Romero R, Yeo L, Gomez-Lopez N, Chaemsaithong P, Jaovisidha A, Gotsch F and Erez O. The etiology of preeclampsia. Am J Obstet Gynecol 2022; 226: S844-S866.
[42] Antar SA, Ashour NA, Sharaky M, Khattab M, Ashour NA, Zaid RT, Roh EJ, Elkamhawy A and Al-Karmalawy AA. Diabetes mellitus: classification, mediators, and complications; a gate to identify potential targets for the development of new effective treatments. Biomed Pharmacother 2023; 168: 115734.
[43] Mistry HD, Ogalde MVH, Broughton Pipkin F, Escher G and Kurlak LO. Maternal, fetal, and placental selectins in women with pre-eclampsia; association with the renin-angiotensin-system. Front Med (Lausanne) 2020; 7: 270.
[44] Kohli S and Blois SM. Platelet-immune cell communication in pregnancy: exploring a new frontier in maternal immunology. J Thromb Haemost 2025; 23: 3791-3795.
[45] Pheiffer C, Dias S, Jack B, Malaza N and Adam S. Adiponectin as a potential biomarker for pregnancy disorders. Int J Mol Sci 2021; 22: 1326.
[46] Al-Naseem A, Sallam A, Choudhury S and Thachil J. Iron deficiency without anaemia: a diagnosis that matters. Clin Med (Lond) 2021; 21: 107-113.
[47] Eisenga MF, Bakker SJ and Gaillard CA. Definition of functional iron deficiency and intravenous iron supplementation. Lancet Haematol 2016; 3: e504.
[48] Kansu-Celik H, Ozgu-Erdinc AS, Kisa B, Findik RB, Yilmaz C and Tasci Y. Prediction of gestational diabetes mellitus in the first trimester: comparison of maternal fetuin-A, N-terminal proatrial natriuretic peptide, high-sensitivity C-reactive protein, and fasting glucose levels. Arch Endocrinol Metab 2019; 63: 121-127.
[49] Mukhopadhyay S, Mondal SA, Kumar M and Dutta D. Proinflammatory and antiinflammatory attributes of fetuin-a: a novel hepatokine modulating cardiovascular and glycemic outcomes in metabolic syndrome. Endocr Pract 2014; 20: 1345-1351.
[50] Chekol Abebe E, Tilahun Muche Z, Behaile T/Mariam A, Mengie Ayele T, Mekonnen Agidew M, Teshome Azezew M, Abebe Zewde E, Asmamaw Dejenie T and Asmamaw Mengstie M. The structure, biosynthesis, and biological roles of fetuin-A: a review. Front Cell Dev Biol 2022; 10: 945287.
[51] Iliodromiti S, Sassarini J, Kelsey TW, Lindsay RS, Sattar N and Nelson SM. Accuracy of circulating adiponectin for predicting gestational diabetes: a systematic review and meta-analysis. Diabetologia 2016; 59: 692-699.
[52] Tao C, Sifuentes A and Holland WL. Regulation of glucose and lipid homeostasis by adiponectin: effects on hepatocytes, pancreatic β cells and adipocytes. Best Pract Res Clin Endocrinol Metab 2014; 28: 43-58.
[53] Han SJ, Fujimoto WY, Kahn SE, Leonetti DL and Boyko EJ. Apolipoprotein B levels predict future development of hypertension independent of visceral adiposity and insulin sensitivity. Endocrinol Metab (Seoul) 2020; 35: 351-358.
[54] Bolatai A, He Y and Wu N. Vascular endothelial growth factor and its receptors regulation in gestational diabetes mellitus and eclampsia. J Transl Med 2022; 20: 400.
[55] Etchegaray-Armijo K, Bustos-Arriagada E, Navarro-Rosenblatt D, Vera C, Garmendia ML, Sobrevia L, López-Alarcón C and Casanello P. Biomarkers of oxidative stress in maternal plasma, umbilical cord and placenta of patients with gestational diabetes: a systematic review and meta-analysis. Free Radic Biol Med 2025; 237: 650-665.